Eur. Phys. J. B **60**, 439–446 (2007)
DOI: 10.1140/epjb/e2008-00016-2

THE EUROPEAN PHYSICAL JOURNAL B

Dynamical behavior of electron transport in AlGaAs/GaAs double-barrier structures under a high-frequency radiation field

Z.H. Dai[1,2,a], J. Ni[2], Y.M. Sun[1], and W.T. Wang[1]

[1] Department of Physics, Yantai University, 264005 Yantai, P.R. China
[2] Department of Physics and Key Laboratory of Atomic and Molecular Nanoscience, Tsinghua University, 100084 Beijing, P.R. China

Received 14 August 2007 / Received in final form 26 November 2007
Published online 16 January 2008 – © EDP Sciences, Società Italiana di Fisica, Springer-Verlag 2008

Abstract. We investigate the time-dependent dynamical behavior of electron transport in AlGaAs/GaAs double-barrier structures under a high-frequency radiation field. The effects of the radiation field with different amplitude and frequency on the real-time and mean current-voltage curves are taken into account. We find that the amplitude and frequency of the radiation field affect the final stable state current-voltage (I-V) behaviors, which leads to the switching between different current states at a smaller bias than that of the absence of the radiation field, and both current hysteresis and resonant peaks are suppressed by the external radiation field. The high radiation field strength can make the resonant peak of current split and the hysteresis of current disappear. This effect provides the potential to use double-barrier structure as a THz photoelectric switch.

PACS. 73.63.Hs Quantum wells – 73.40.Gk Tunneling – 73.23.-b Electronic transport in mesoscopic systems – 72.10.Bg General formulation of transport theory

1 Introduction

It is well known that double-barrier resonant tunneling nanostructures have been extensively studied due to their various potential device applications and their significance in the study of confined structures [1,2]. There are many important experimental researches, which include the observation of the intrinsic tristability [3], the spatial variation of the quantum-well wavefunction [4], spin-split states [5], and excitonic dark states in the quantum well [6]. Most of experimental researches on the dc transport have been studied, such as the linear and nonlinear response as well as the time-response and the carrier leakage phenomena [7–9]. Three features appeared in the current-voltage (I-V) curves of double-barrier devices in experiments: i) a negative differential resistance has been found in all double barrier structures; ii) a hysteretic plateaulike structure of current is found after the bias passes the resonant value in some experiments [10,11]; iii) Three types of current bistabilities have been found, i.e. single bistability occurring before the current resonant peak [12–15], single bistability after the current resonant peak [16–18], and the double bistabilities and hystereses [19–21]. To explain the bistability and hysteresis phenomena, there are various theoretical models. Both the bistability and the hysteresis in the I-V curve are theoretically explained, their reason are due to the electrostatic feedback caused by the space-charge buildup in the quantum well(QW) [22] as well as a phenomenological LRC model caused by the current oscillations [23,24]. Later numerical simulations suggested that there is an intrinsic high frequency oscillation of current associated with the coupling between the central and the emitter quantum well formed under the bias, which affects the current bistability and plateaulike structures [25,26]. We also use numerical simulation techniques with the large position and momentum discrete meshes to study the microscopic physical mechanism of two bistabilities and hysteresis, and give a perfect and rational explanation [27,28].

Recently, there has been a rapid development of the tunable high frequency switching semiconductor device. Sollner et al. estimated that the resonant tunnelling structure would have picosecond switching time [29]. The resonant tunnelling at an infra-red radiation and an ac electric field have been studied [30–32], photoelectric behaviors in these double-barrier structures have also been studied in experiments [33–35]. Subsequently, Cao et al. investigated the nonlinear absorption of the terahertz radiation in double-barrier resonant structures as well as the superlattice structure in experiments [36–39]. Especially,

[a] e-mail: zhdai@ytu.edu.cn

Orellana et al. studied the dynamic instability induced by the magnetic and the terahertz laser and provided an advice of using the double-barrier structure as a picosecond switching under the intense terahertz laser [40–43]. These time-dependent nonlinear characteristics in double-barrier structures may have the potential applications in the future high-frequency and switching devices. According to our foregoing studies [44], we find that the effect of the time-dependent transient current and charge density variations in the case of the radiation field are very important, and a detailed theoretical study on the radiation filed is necessary.

In this paper, using the time-dependent self-consistent Wigner-Poisson transport model, we study I-V features of an AlGaAs/GaAs/AlGaAs double-barrier structure under the radiation field with different amplitude and frequency. We consider their effects on the electronic charge density distribution and the electron motion. The previous studies about the switching device aim at the bistability region caused by two charge buildup states in the quantum well [33,41–43], whose response time is larger than 2 ps. Now we find the switching effect in the other bistabilty region, i.e., current hysteresis region, caused by the current oscillations. This region has shorter switching response time and larger sensitivity to the external radiation field.

This paper is organized as follows: In Section 2, we briefly describe the numerical technique used in this paper. The numerical results and discussion about the time-dependent current transport and local electron distribution are presented in Section 3. The conclusion of this paper is given in Section 4.

2 Methods

In the simulation of the double-barrier structure, there are two kinds of methods to be used. The first is the Monte Carlo method [45–47], which is based on the quantum statistical method. The second is based upon physical transport equations, which include directly solving transport equation [48–52] and the self-consistent transport-Poisson equation [53–57], and the later more affects the actual device. Here, we use time-dependent self-consistent Wigner-Poisson equation in our simulation of nanodevices.

We consider an AlGaAs/GaAs/AlGaAs double-barrier structure. The original potential difference between the emitter and collector is roughly proportional to the total voltage drop V across the device. The used potential is the self-consistent result from the Wigner function equation (WFE) and Poisson equation (PE). The Wigner function formulation of the quantum transport has been used to study the electron transport in nanodevices [59,58]. It has many useful characteristics in the simulation of quantum-effect electronic devices, including the ability to handle dissipated and open-boundary systems naturally. With the lowest-order approximation to the scattering, the time-dependent dynamic equation for quantum transport is given by

$$\frac{\partial f(x,k)}{\partial t} = -\frac{\hbar k}{m^*}\frac{\partial f(x,k)}{\partial x} - \frac{1}{\hbar}\int_{-\infty}^{\infty}\frac{dk'}{2\pi}(f(x,k') \times V(x,k-k')) + \left.\frac{\partial f(x,k)}{\partial t}\right|_{coll}, \quad (1)$$

where the kernel of the potential operator

$$V(x,k-k') = \int_{-L/2}^{L/2} dr \sin[(k-k')r] \times [U(x+r/2) - U(x-r/2)] \quad (2)$$

m^* is the electron effective mass, x and r is the Wigner-Weyl transformation coordinate [59], and U is the conduction-band edge. $f(x,k)$ is the Wigner function, which is defined as

$$f(x,k) = \int dr\, \rho(x+r/2, x-r/2)\exp(-ikr), \quad (3)$$

where ρ is the electron density operator. Appropriately treating scattering in semiconductors is very important for getting reasonable simulation results. Recent research shows that the computation burden associated with the detailed consideration of electron-phonon scattering is formidable. The amount of computation time would be too huge if we treat the scattering in detail. Thus, we employ the relaxation-time approximation to deal with the scattering in this paper. In terms of the relaxation time approximation to scattering, the collision term in the above equation may be written as [25]

$$\frac{\partial f(x,k)}{\partial t} = \frac{1}{\tau}\left[\frac{f_0(x,k)}{\int f_0(x,k)\,dk}\int f(x,k)\,dk - f(x,k)\right], \quad (4)$$

where τ is the relaxation time and f_0 is the equilibrium Wigner function. The boundary conditions are

$$f(-L/2,k)\,|_{k>0} = \frac{m^* k_B T}{\pi\hbar^2} \times \ln\left\{1 + \exp\left[-\frac{1}{k_B T}\left(\frac{\hbar^2 k^2}{2m^*} - \mu_L\right)\right]\right\}, \quad (5)$$

$$f(L/2,k)\,|_{k<0} = \frac{m^* k_B T}{\pi\hbar^2} \times \ln\left\{1 + \exp\left[-\frac{1}{k_B T}\left(\frac{\hbar^2 k^2}{2m^*} - \mu_R\right)\right]\right\}. \quad (6)$$

The Poisson equation is

$$\frac{d^2}{dx^2}u(x) = \frac{q^2}{\varepsilon}\left[N_d(x) - n(x)\right], \quad (7)$$

where ε is the dielectric permittivity, $u(x)$ is the electrostatic potential, q is the electronic charge, $N_d(x)$ is the concentration of ionized dopants, and $n(x)$ is the density of electrons, which is given by

$$n(x) = \int_{-\infty}^{\infty}\frac{dk}{2\pi}f(x,k). \quad (8)$$

The corresponding current density may be written as

$$j(x) = \int_{-\infty}^{\infty} \frac{dk}{2\pi} \frac{\hbar k}{m^*} f(x,k). \tag{9}$$

To solve the WFE-PE equations, we must discretize the simulation zone of the WFE-PE equation. The details of the discretization of the WFE are described by Frensley and Jensen et al. [25,59].

The time-dependent WFE can be written as

$$\frac{\partial f}{\partial t} = \frac{\Xi}{i\hbar} f, \tag{10}$$

where operator Ξ is given by

$$\Xi = i(T + V + S). \tag{11}$$

T, V, and S are the drift, potential, and scattering terms, respectively. The solution of this equation is

$$f(t+\delta t) = \exp\left(-\frac{i\Xi}{\hbar}t\right) f(t) = \frac{1 - \frac{i\Xi}{2\hbar}t}{1 + \frac{i\Xi}{2\hbar}t}. \tag{12}$$

The equation may be written as

$$[-2\hbar/\delta t + \Xi]\,[f(t+\delta t) + f(t)] = -4\hbar f(t)/\delta t. \tag{13}$$

In the discretized equation, the drift term gives the boundary condition, which does not change with time. Thus, we have

$$\left[-2\hbar/\delta t + \tilde{\Xi}\right][f(t+\delta t) + f(t)] = -4\hbar f(t)/\delta t + 2BC, \tag{14}$$

where $\tilde{\Xi}$ is the operator defined by equation (12) without considering the boundary conditions of the Wigner function, BC is the boundary condition. In the whole calculation, we neglect the differences of the dielectric function and the effective mass of electrons in the different region of the device.

PE is a highly nonlinear equation and the discretization of the PE is trivial. It is not suitable to directly solve this equation in the iterative Wigner-Poisson equations. The detailed treatment about discretizing PE in the device space domain can be found in reference [60].

In our simulations, we first approximate the conduction-band profile by a square well potential, the effect of the external electromagnetic radiation field is taken into account by time-dependent ac voltage which is dependent on the spacial position of simulation device [31], i.e., it includes a bias voltage $Am\frac{qx}{L}\sin(2\pi\nu t)$ on the device along the growth direction, where Am and $\nu = \frac{1}{T}$ are the amplitude and frequency of the radiation field, respectively, and L is simulation device length. For the double-barrier structure, the total time-dependent potential can be written as $u(x,t) = U_{dc} + Am\frac{qx}{L}\sin(2\pi\nu t)$. Applying this time-dependent potential $u(x,t)$ to each iteration of the transient Wigner-Poisson coupling equation and get $n(x)$ from equations (1) and (8). The density of electrons is substituted into the Poisson equation and then the new conduction-band profile

$$U(x,t) = u(x,t) + \Delta_c(x) \tag{15}$$

is obtained, where $\Delta_c(x)$ is the offset of the band edge. Using this new conduction-band profile at the next time simulation step, and each time simulation step is 4 fs, which is valid in simulating THz ultrafast region. In each time simulation step, we consider the effect of the acoustic phonon, piezoelectric phonon, zero order optical phonon, polar optical phonon and ionized impurity, through these effects on the dissipated term we adjust the electron-phonon interaction term to give total relaxation time. With the increase of the time simulation step, the Wigner function equation is solved again. The iteration process continues until a steady-state or a preassigned time value are achieved by a simultaneous solution of both equations (1) and (7).

3 Numerical results and discussion

We have calculated the time-dependent electron transport in the double-barrier structure using the transient Wigner-Poisson transport method. The parameters used in our simulation are as follows. The momentum and position spaces are broken into 72 and 86 points, respectively. The donor density is $N_d = 2.0 \times 10^{18}$ /cm^3 and the quantum well and barrier regions are undoped. The compensation ratio for scattering calculations is 0.3, and the barrier and quantum well widths are 3 and 5 nm, respectively. The simulation box length is 55 nm, and the barrier potential is 317 meV. The device temperature is 77 K, and the effective mass of an electron is assumed to be constant and equals 0.0667 m_0. The doping region extends to 3 nm before the emitter barrier and after the collector barrier.

In order to study the effect of the radiation field on the transport properties of the double-barrier structure, we first give the mean current density through the double-barrier structure under the radiation field with different amplitudes Am and a fixed period of $T = 400$ fs. When the time-dependent simulation reaches steady state in the forward and backward bias sweeps (FBS and BBS), *I-V* behaviors of the resonant tunneling structure are shown in Figure 1. Compared to the zero and the low radiation field, as shown in Figures 1a–1c shows that the extent of the current plateaulike structure under the 10 meV radiation field is very narrow and the current peak is also depressed. When the amplitude of the radiation field is further increased, as shown in Figure 1d, where the amplitude of the radiation field is 50 mV, we show that the current plateaulike structure disappears and the original current peak value is splitted into several peaks. In order to explain the depression of the current plateaulike structure and current peak, we will give the time-dependent current and the local electron density distributions.

Figures 2a–2d give the time-dependent current change in the different bias voltage. Under the zero radiation field shown in Figure 2a, the current density shows oscillations

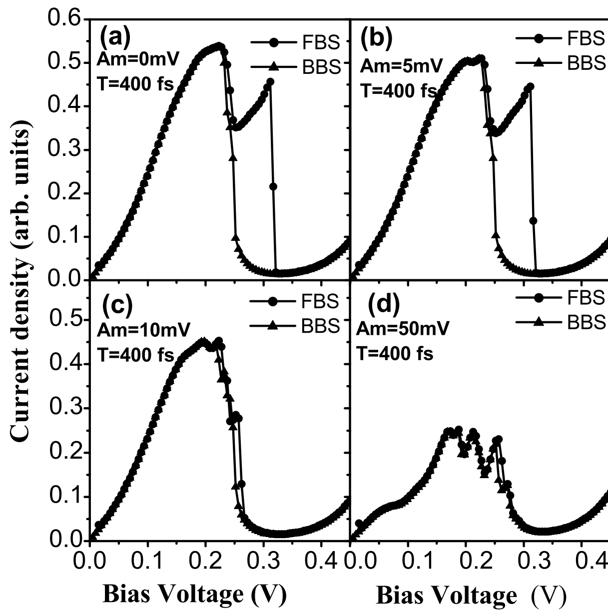

Fig. 1. *I-V* curves of the double-barrier structure irradiated by the different radiation field amplitude with a period T=400 fs. The data are the time average value of current oscillation taken from the steady states of the simulation in the forward and backward bias sweep (FBS and BBS) process. Figures 1a–1d correspond to the radiation field under $Am = 0$ mV, 5 mV, 10 mV and 50 mV, respectively.

after the bias passes the position where the resonant peak value of current appears, whose intrinsic oscillation period is about 400 fs. This current oscillation prevents the decrease of the mean current, and the mean current shows a plateaulike structure shown in Figure 1a. The current oscillation is due to the coupling of the energy level in the emitter and main quantum well [26–28]. The radiation field affects this coupling mechanism, especially under the higher radiation field strength (10 mV). Figure 2c shows that the strong external radiation field makes the intrinsic oscillation of current irregular and leads to the collapse of the current plateaulike structure in a smaller bias voltage. But Figure 2b shows that the low radiation field does not destroy the current oscillation. With the increase of the amplitude of the radiation field, the external radiation field influences the original *I-V* behavior and leads to the complete destroy of the coupling of the energy levels. Here, the current plateaulike structure disappears and the current peak shows splitting, as shown in Figure 2d.

In fact, the changes of *I-V* behaviors are finally due to the changes of the local electron distribution under the external radiation field. In the situation of the zero radiation field, the electron density distribution before the emitter barrier shows an evident exhausted layer after the bias passes the position of the resonant peak value of current, which maintains in a window of the bias sweep, as shown in Figure 3a. In this special window of the bias sweep, the changes of the local electron density distribution will lead to an emitter quantum well in the potential structure, and the coupling of energy level between the emitter

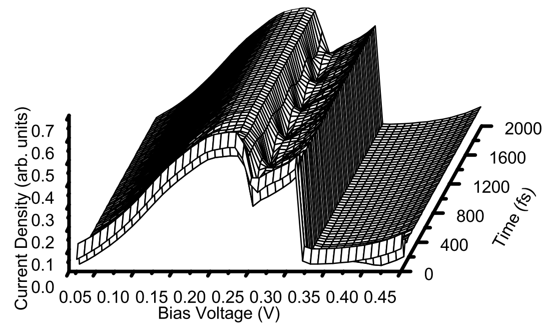

(a)

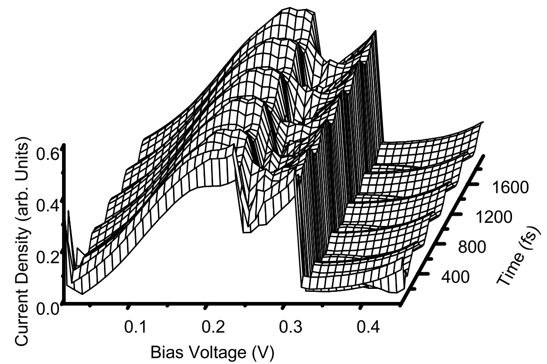

(b)

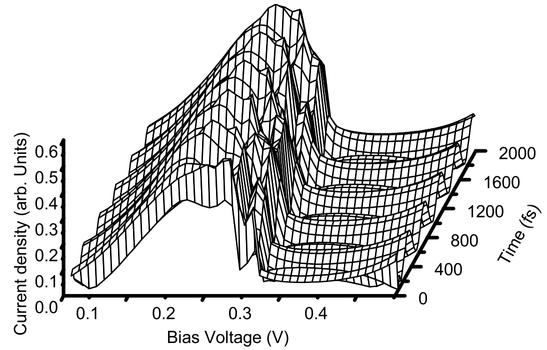

(c)

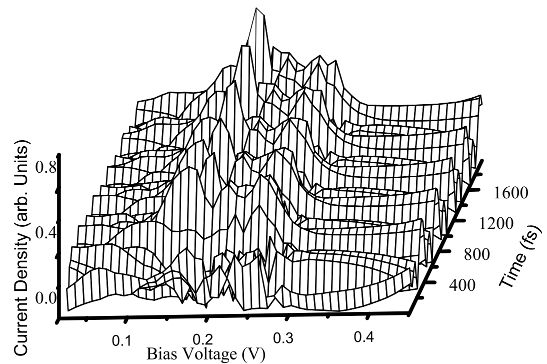

(d)

Fig. 2. The time-dependent current features of double-barrier structures with bias voltages as parameters for the case of the forward bias sweep process. Figures 2a–2d correspond to the radiation field under $Am = 0$ mV, 5 mV,10 mV and 50 mV, respectively.

and the main quantum well prevents the decrease of the quasi-bound state in the main quantum well. The mean current shows a plateaulike structure in this window of the bias sweep. The external radiation field affects the electron density redistribution. When the amplitude of the radiation field is 5 mV, as shown in Figure 3b, the radiation field does not evidently change the electron distributions. However, with the increase of the amplitude of the radiation field, Figure 3c shows that the window of the bias sweep, where the local electron density before the emitter barrier shows the exhausted layer and the potential shows the emitter quantum well, become narrower. Finally when the amplitude of the radiation field is large enough, the exhausted layer of the electron density before the emitter barrier disappears and thus leads to the disappearance of the emitter quantum well completely. It should be noted that Figure 3d shows that the electron density in the main well splits into several peaks, which leads to the splitting of mean current peak values in Figure 1d.

From above discussions, we know that the amplitude of the radiation field significantly affects the I-V behavior of the double-barrier structure and the large radiation field leads to the current plateaulike structure collapse at a smaller bias than that in the absence of the external radiation field. In order to further study the effect of the amplitude of the radiation field on the current plateaulike structure, Figure 4 a gives the I-V curves under different amplitudes of the radiation field with a period of 400 fs. From the figure, we can see that in the case of the small radiation field ($Am = 3$ and 5 mV), the whole I-V curve is not changed, and the current plateaulike structure ends at the bias 0.311 mV. When the amplitude of the radiation field arrives 7 mV, the current plateaulike structure collapses in the bias 0.287 mV. With the amplitude of the radiation field arrives to 10 mV, the original current plateaulike structure is changed completely. The start point of the bias, where the current decrease after the resonant value, decrease and the extent of the current plateaulike structure is very narrow. The effect of the radiation field on the current oscillation can be found in Figure 4b. From the figure, we can see that under the smaller amplitude of the radiation field, the oscillation amplitude of current is increased, as shown in the case of $Am = 3$ and 5 mV. However, the larger amplitude of the radiation field destroys the original intrinsic oscillation frequency of current, as shown in the case of $Am = 7$ and 10 mV.

Now we consider the effect of the frequency of the radiation field on the electron transport, the results are shown in Figure 5a. The frequency of the external radiation field plays an important role on the current plateaulike structure. In the backward bias sweep, the effect of the radiation field on the I-V curve is not significant. We mainly give the results of the forward bias sweep process. In the device we considered, the intrinsic oscillation period in the hysteresis region is about 400 fs, so we consider the frequency of the radiation field close to this value. We call the radiation field whose oscillation frequency above 400 fs the high frequency, in verse, is the low frequency field, In the situation of 5 mV radiation field, the high

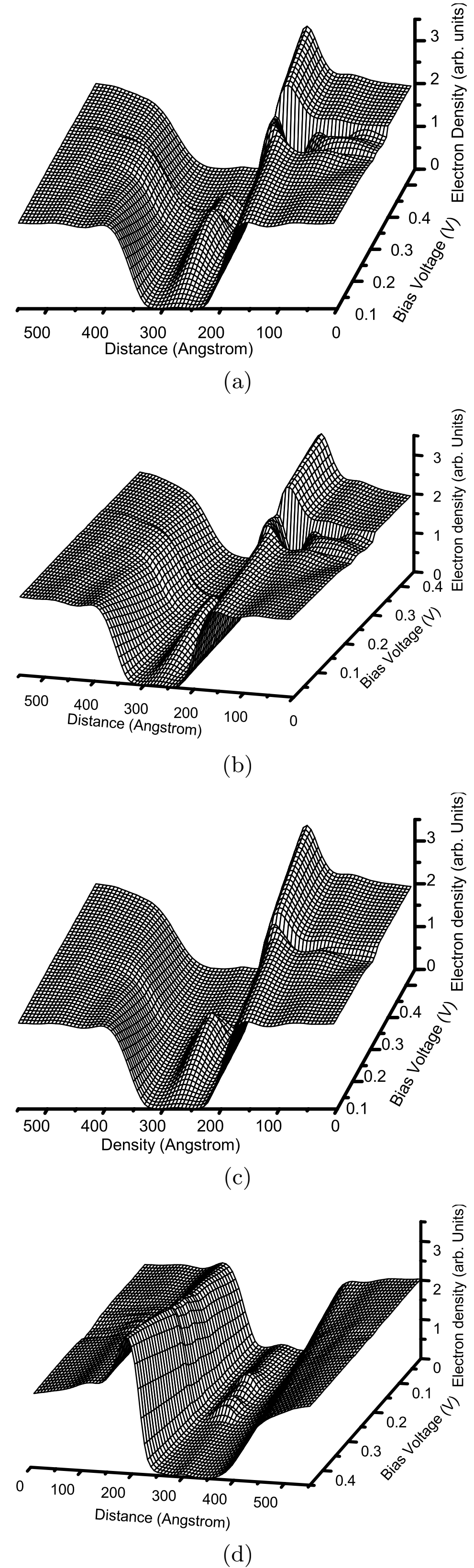

Fig. 3. The local electron density distribution with bias voltages as parameters for the case of forward bias sweep process. Figure a–d correspond to the radiation field under Am=0 mV, 5 mV, 10 mV and 50 mV, respectively.

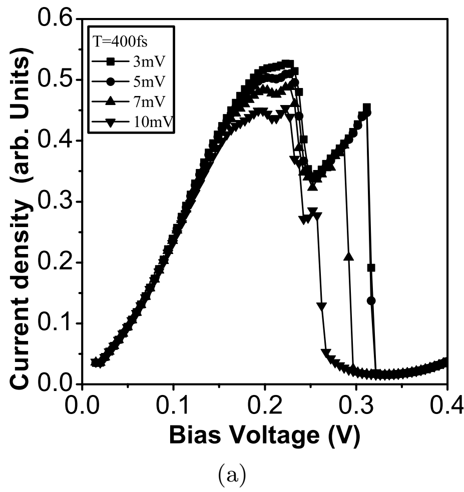

(a)

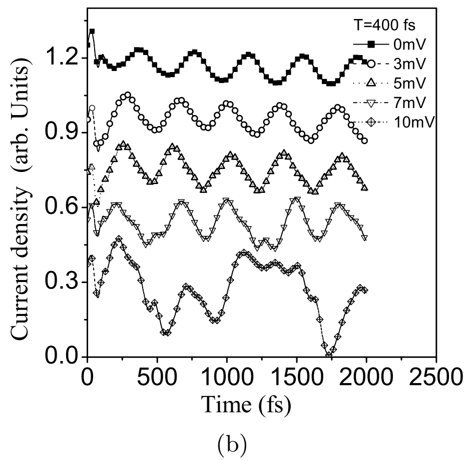

(b)

Fig. 4. I-V curves of the double-barrier structures irradiated by different radiation field amplitude Am with a constant period $T = 400$ fs for the case of the forward bias sweep process. Figure 4b show the corresponding time-dependent current density curves for the different radiation field amplitude Am.

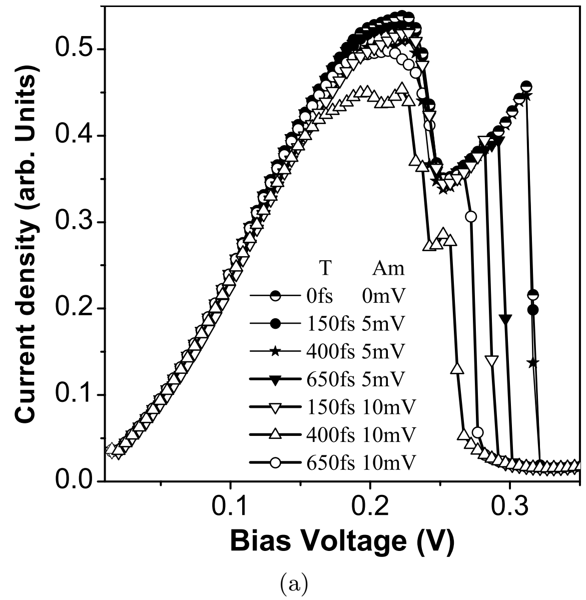

(a)

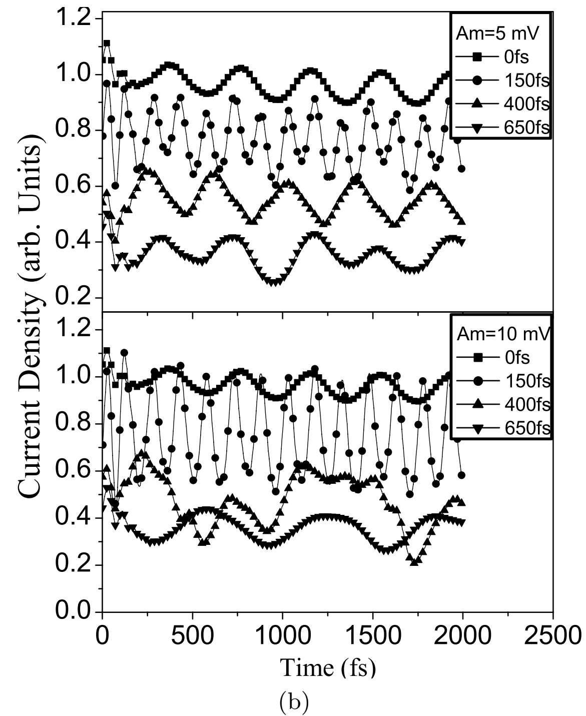

(b)

Fig. 5. I-V curves of the double-barrier structure irradiated by different radiation field amplitude Am with a different period $T = 150, 400$, and 650 fs for the case of the forward bias sweep process. Figure 5b is the corresponding time-dependent current density curve for the different radiation field amplitude Am and frequency T.

frequency radiation field prevents the collapse of the current plateaulike structure. But when the frequency of the radiation field is below the original oscillation frequency, the current plateaulike structure will end in a smaller bias. For the 10 mV radiation field, we also find an abnormal phenomenon. When the radiation field frequency is close to the intrinsic frequency of the device, the start point of the bias, where the current shows plateaulike structure, is decreased. The reason is that in these amplitudes and frequencies of the radiation field, the I-V curves have already been decreased in a smaller bias position. This phenomenon has also been found in the case of 5 mV radiation field. Because it's effect is very small and does not make a large change on the final I-V curves. The effects of the amplitude and frequency of the radiation field on the transient current are shown in Figure 5b. From the figure, we can see that the high frequency radiation field modulates only the current intrinsic frequency and does not lead to the basic destroy of the mean current value. But the low frequency radiation field has destroyed the intrinsic oscillations and caused the current plateaulike structure collapse in a smaller bias. This can be seen very clearly from the time-dependent I-V curve shown in Figures 6a and 6b. Figures 7a and 7b show that this effect on the mean current is mainly due to the change of the local electron distribution under the radiation field. From above discussions, we can see that the amplitude and frequency

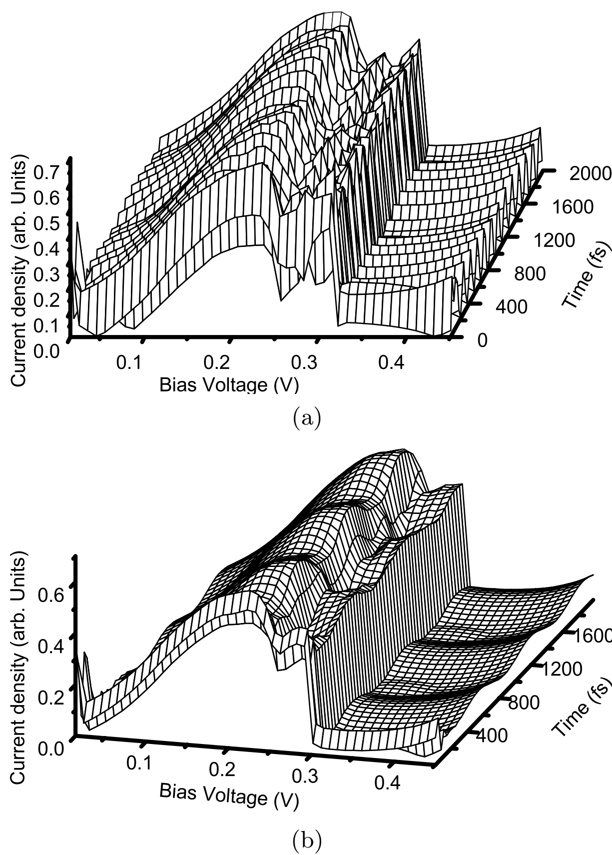

Fig. 6. The time-dependent current characteristics of double-barrier structures under 5 mV radiation field for the case of the forward bias sweep. (a) the radiation field frequency of 150 fs, (b) the radiation field frequency of 650 fs.

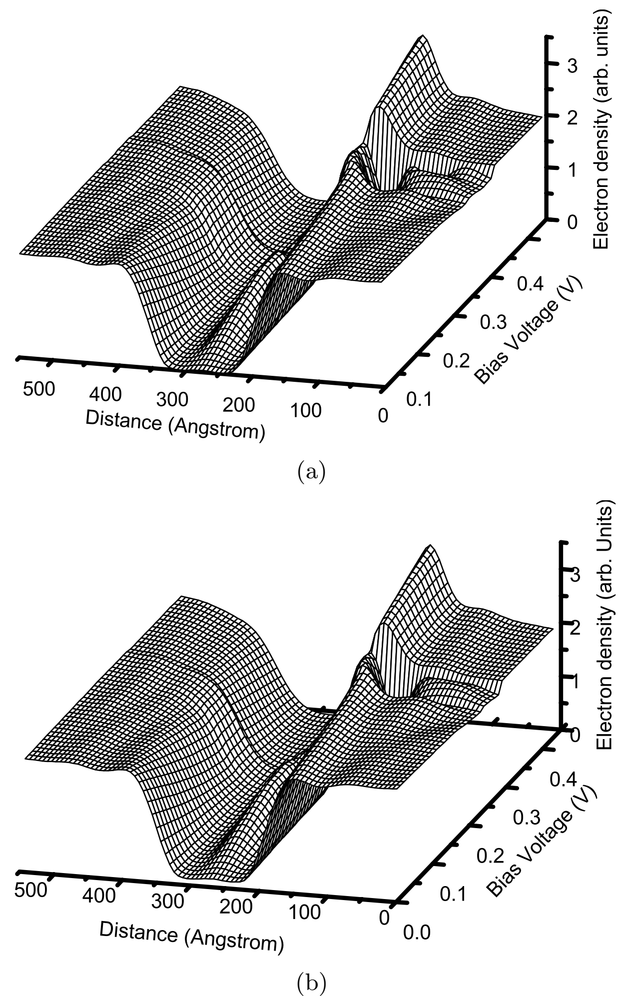

Fig. 7. The local electron density distribution of double-barrier structures under 5 mV radiation field for the case of the forward bias sweep. (a) the radiation field frequency of 150 fs, (b) the radiation field frequency of 650 fs.

of the radiation field can affect the switching of the current hysteresis. This effect can be used to make a photo-electronic switch in the hysteresis region and can also be used to change the width of the current hysteresis region.

4 Conclusion

We have numerically solved the time-dependent coupled Wigner-Poisson equation for the double-barrier structure under the radiation field. The amplitude and frequency of the radiation field affect strongly the electron density distribution and the mean current. The radiation field damps the formation of the exhausted layer of electron density and thus affects the formation of the potential well in the emitter region. The distributions of electron density and emitter quantum well further affect the current oscillation and plateaulike structure. Therefore, the radiation field leads to the plateaulike structure of the current collapse in a smaller bias than that of the absence of the radiation field. By using the radiation field, we can adjust the different degree of current hysteresis in the double-barrier structure device. Using this technique, we can make a new light-operated switch device in the bistability region after the resonant bias value, which has the higher sensitivity and the controllable property than that in the bistability region before the resonant bias value.

The work was supported by the National Foundation of Natural Science in China (Grants No 10404022) and the Natural Science Foundation of Shandong province of China (Grants No Y2006A25).

References

1. Y.V. Nazarov, L.I. Glazman, Phys. Rev. Lett. **91**, 126804 (2003)
2. J.C. Blakesley, P. See, A.J. Shields, B.E. Kardynal, P. Atkinson, I. Farrer, D.A. Ritchie, Phys. Rev. Lett. **94**, 067401 (2005)
3. A.D. Martin, M.L.F. Lerch, P.E. Simmonds, L. Eaves, Appl. Phys. Lett. **64**, 1248 (1994)
4. R.K. Kawakami, E. Rotenberg, H.J. Choi, E.J. Escorcia-Aparicio, M.O. Bowen, J.H. Wholfe, E. Arenholz, Z.D. Zhang, N.V. Smith, Z.Q. Qiu, Nature **398**, 132 (1999)

5. D. Grundler, Phys. Rev. Lett. **84**, 6074 (2000)
6. D. Snoke, S. Denev, Y. Liu, L. Pfeiffer, K. West, Nature **418**, 754, (2002)
7. S.Q. Murphy, J.P. Eisenstein, L.N. Pfeiffer, K.W. West, Phys. Rev. B **52**, 14825 (1995)
8. N. Tansu, Jeng-Ya Yeh, Luke J. Mawst, Appl. Phys. Lett. **83**, 2112 (2003)
9. T. Ohtsuka, L. Schrottke, R. Hey, H. Kostial, H.T. Grahn, J. Appl. Phys. **94**, 2192 (2003)
10. M. Giltrow, A. Kozorezov, M. Sahraoui-Tahar, J.K. Wigmore, J.H. Davies, C.R. Stanley, B. Vogel, C.D.W. Wilkinson, Phys. Rev. Lett. **75**, 1827 (1995)
11. T. Reker, H. Im, L.E. Bremme, H. Choi, Y. Chung, P.C. Klipstein, H. Shtrikman, Phys. Rev. Lett. **88**, 056403 (2002)
12. M.L. Leadbeater, E.S. Alves, F.W. Sheard, L. Eaves, M. Henini, O.H. Hughes, G.A. Toombs, J. Phys.: Condens. Matter **1**, 10605 (1989)
13. B. Su, V.J. Golman, M. Santos, Shayegan, Appl. Phys. Lett. **58**, 747 (1991)
14. C.R. Wie, Y.W. Choi, Appl. Phys. Lett. **58**, 1077 (1991)
15. L.D. Macks, S.A. Brown, R.G. Clark, R.P. Starrett, M.A. Reed, M.R. Deshpande, C.J.L. Fernando, W.R. Frensley, Phys. Rev. B **54**, 4857 (1996)
16. O.H. Hughes, M. Henini, E.S. Alves, L. Eaves, M.L. Leadbeater, T.J. Foster, F.W. Sheard, G.A. Toombs, A. Celeste, J.C. Portal, J. Vac. Sci. Technol. B **6**, 1161 (1988)
17. V.J. Goldman, D.C. Tsui, J.E. Cunningham, Phys. Rev. B **36**, 7635 (1987)
18. T.J. Foster, M.L. Leadbeater, L. Eaves, M. Henini, O.H. Hughes, C.A. Payling, F.W. Sheard, P.E. Simmonds, G.A. Toombs, G. Hill, M.A. Pate, Phys. Rev. B **39**, 6205 (1989)
19. L. Eaves, G.A. Toombs, F.W. Sheard, C.A. Payling, M.L. Leadbeater, E.S. Alves, T.J. Foster, P.E. Simmonds, M. Henini, O.H. Hughes, J.C. Portal, G. Hill, M.A. Pate, Appl. Phys. Lett. **52**, 212, (1988)
20. T.C.L.G. Sollner, Phys. Rev. Lett. **59**, 1622 (1987)
21. V.J. Goldman, D.C. Tsui, J.E. Cunningham, Phys. Rev. Lett. **58**, 1256 (1987), Phys. Rev. Lett. **59**, 1623 (1987)
22. F.W. Sheard, G.A. Toombs, Appl. Phys. Lett. **52**, 1228 (1988)
23. E.R. Brown, C.D. Parker, T.C.L.G. Sollner, Appl. Phys. Lett. **54**, 934 (1989)
24. H.C. Liu, Appl. Phys. Lett. **53**, 485 (1988)
25. K.L. Jensen, F.A. Buot, Phys. Rev. Lett. **66**, 1079 (1991)
26. Peiji Zhao, H.L. Cui, D.L. Woolard, Phys. Rev. B **63**, 075302 (2001)
27. Zhenhong Dai, Jun Ni, Phys. Lett. A **342**, 272 (2005)
28. Zhenhong Dai, Jun Ni, Phys. Rev. B **73**, 115611 (2006)
29. J.F. Whitaker, G.A. Mourou, T.C.L.G. Sollner, W.D. Goodhue, Appl. Phys. Lett. **53**, 385 (1988)
30. V.A. Chitta, C. Kutter, R.E.M. de Bekker, J.C. Maan, S.J. Hawksworth, J.M. Chamberlain, M. Henini, G. Hill, J. Phys.: Condens. Matter **6**, 3945 (1994)
31. R. Aguado, J. Inarrea, G. Platero, Phys. Rev. B **53**, 10030 (1996)
32. F. Grossmann, Phys. Rev. B **70**, 113306 (2004)
33. C. Zhang, Appl. Phys. Lett. **78**, 4187 (2001)
34. Der-Feng Guo, J. App. Phys. **91**, 672 (2002)
35. X.G. Peralta, S.J. Allen, M.C. Wanke, N.E. Harff, J.A. Simmons, M.P. Lilly, J.L. Reno, P.J. Burke, J.P. Eisenstein, Appl. Phys. Lett. **81**, 1627 (2002)
36. J.C. Cao, X.L. Lei, Phys. Rev. B **59**, 2199 (1999)
37. H.C. Liu, C.Y. Song, Z.R. Wasilewski, A.J. Spring Thorpe, J.C. Cao, C. Dharma, G.C. Aers, D.J. Lockwood, J.A. Gupta, Phys. Rev. Lett. **90**, 077402 (2003)
38. J.C. Cao, Phys. Rev. Lett. **91**, 237401 (2003)
39. H.C. Liu, C.Y. Song, A.J. Spring Thorpe, J.C. Cao, Appl. Phys. Lett. **84**, 4068 (2004)
40. P. Orellana, E. Anda, F. Claro, Phys. Rev. Lett. **79**, 1118 (1997)
41. P. Orellana, E. Anda, F. Claro, Appl. Phys. Lett. **75**, 1643 (1999)
42. P. Orellana, F. Claro, E. Anda, Phys. Rev. B. **62**, 9959 (2000)
43. P. Orellana, F. Claro, Phys. Rev. Lett. **90**, 178302 (2003)
44. Zhenhong dai, Jun Ni, Appl. Phys. Lett. **88**, 192107 (2006)
45. H. Callebaut, S. Kumar, B.S. Williams, Qing Hu, J.L. Reno, Appl. Phys. Lett. **84**, 645 (2004)
46. P. Delaney, J.C. Greer, Phys. Rev. Lett. **93**, 036805 (2004)
47. A. Reklaitis, Appl. Phys. Lett. **86**, 262110 (2005)
48. C.L. Fernando, W.R. Frensley, Phys. Rev. B **52**, 5092 (1995)
49. G. Klimeck, R. Lake, R.C. Bowen, W.R. Frensley, T.S. Moise, Appl. Phys. Lett. **67**, 2539 (1995)
50. I. Lapushkin, A. Zakharova, V. Gergel, H. Goronkin, S. Tehrani, J. Appl. Phys. **82**, 2421 (1997)
51. A. Patane, A. Polimeni, L. Eaves, P.V.C. Main, M. Henini, A.E. Belyaev, Yu.V. Dubrovskii, P.N. Brounkov, E.E. Vdovin, Yu.N. Khanin, G. Hill, Phys. Rev. B **62**, 13595 (2000)
52. R. Gebauer, R. Car, Phys. Rev. B **70**, 125324 (2004)
53. Y. Fu, M. Willander, J. Appl. Phys. **73**, 1848 (1993)
54. J.M. Bigelow, J.P. Leburton, J. Appl. Phys. **76**, 2887 (1994)
55. K.L. Jensen, F.A. Buot, J. Appl. Phys. **67**, 2153 (1990)
56. P. Bordone, M. Pascoli, R. Brunetti, A. Bertoni, C. Jacoboni, A. Abramo, Phys. Rev. B **59**, 2060 (1999)
57. C. Rivas, R. Lake, W.R. Frensely, G. Klimeck, P.E. Thompson, K.D. Hobart, S.L. Rommel, P.R. Berger, J. Appl. Phys. **94**, 5005 (2003)
58. R.P. Zaccaria, F. Rossi, Phys. Rev. B **67**, 113311 (2003), R.P. Zaccaria, F. Rossi, Semicond. Sci. Technol. **19**, S257 (2004)
59. W.R. Frensley, Rev. Mod. Phys. **62**, 745 (1990)
60. Zhenhong Dai, Jun Ni, Eur. Phys. J. B **45**, 129 (2005)